CHAPTER 3

RESULTS AND DISCUSSIONS

3.1 Synthesis and characterization of polymeric salens containing glycolic chain (7, 8 and 9).

All the polymeric salens containing flexible glycolic chains were synthesized according to Scheme 3.1. In the first step, ditosylated compounds were prepared through tosylation of the corresponding glycols with tosylchloride. The nucleophilic substitution of the ditosylates with 2,4-dihydroxybenzaldehyde afforded the desired dialdehyde monomers. The final polymerization step was performed using condensation reaction between the dialdehyde monomers and 1,2 diaminocyclohexane to give the targeted polymers.

The tosylation of diethylene glycol with 2 equivalents of tosylchloride in dichloromethane as a solvent gave white needle-like crystal of ditosylate **1** (67% yield) after precipitation in dichloromethane and ether. The ^{1}H-NMR spectrum of **1** (Figure 3.1) showed doublet of doublet signals of aromatic proton (Ar**H**) at 7.35 and 7.76 ppm and singlet signal of methyl protons (Ar**CH**$_3$) at 2.43 ppm instead of the broad signal of hydroxylic protons at 4.39 ppm (**HO**CH_2CH_2O) found in the spectrum of the starting diethyleneglycol.

Like the ditosylated ester of diethylene glycol (**1**) , the ditosylated ester of tri- and tetraethyleneglycol (**2** and **3**) were prepared by the similar procedure that gave white needle-like crystal of ditosylate ester **2** and colorless oil of ditostylated ester **3** in 73% and 71% respectively.

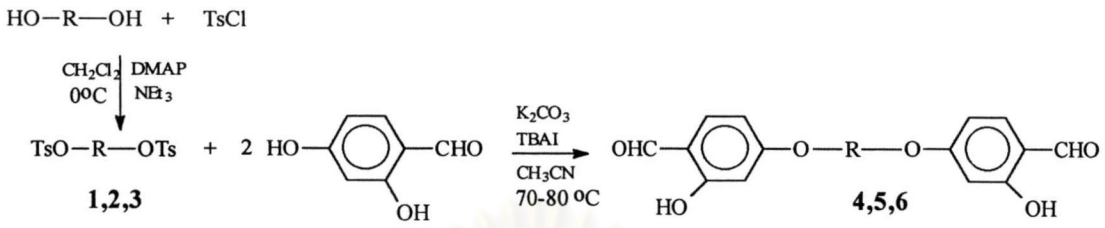

1, R = $CH_2CH_2OCH_2CH_2$, 67 % yield

2, R = $CH_2CH_2OCH_2CH_2OCH_2CH_2$, 73 % yield

3, R = $CH_2CH_2OCH_2CH_2OCH_2CH_2OCH_2CH_2$, 71 % yield

4, R = $CH_2CH_2OCH_2CH_2$, 58 % yield

5, R = $CH_2CH_2OCH_2CH_2OCH_2CH_2$, 32 % yield

6, R = $CH_2CH_2OCH_2CH_2OCH_2CH_2OCH_2CH_2$, 13 % yield

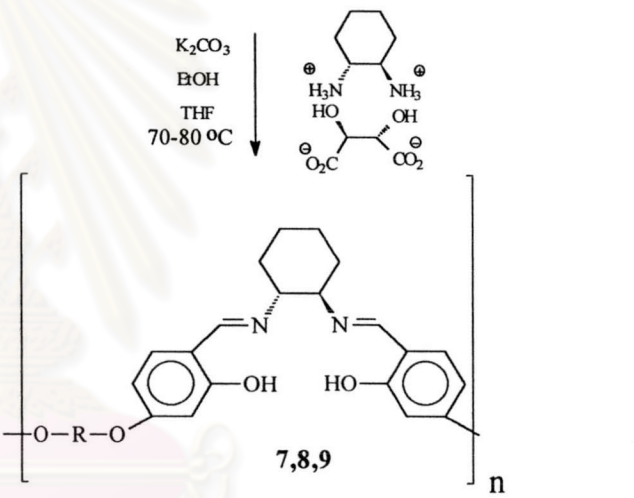

7, R = $CH_2CH_2OCH_2CH_2$, 79 % yield

8, R = $CH_2CH_2OCH_2CH_2OCH_2CH_2$, 81 % yield

9, R = $CH_2CH_2OCH_2CH_2OCH_2CH_2OCH_2CH_2$, 83 % yield

Scheme 3.1. Synthetic pathway of polymeric salens containing flexible glycolic chains.

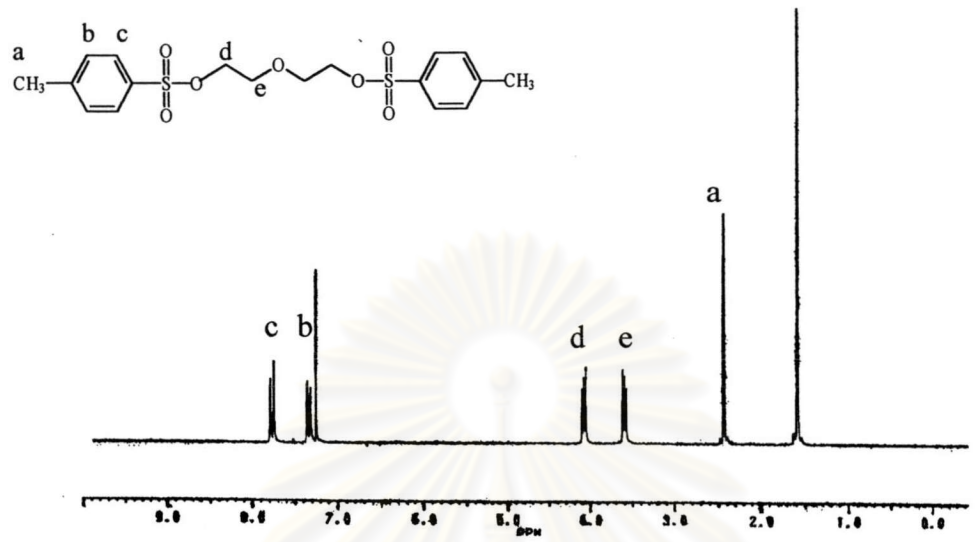

Figure 3.1 The ^{1}H-NMR spectrum of tosylate ester of diethyleneglycol, **1**

The double nucleophilic substitution reaction of the ditosylates with 2,4-dihydroxybenzaldehyde gave the corresponding dialdehyde products (**4**, **5** and **6**) in 58%, 32% and 13% yield, respectively. Typically, 2 equivalents of 2,4-dihyldroxybenzaldehyde was mixed with 1 equivalent of ditosylate **1** in acetonitrile in the presence of 1 equivalent of K_2CO_3 as a base and 10% of tetrabutylammonium iodide as a phase-transfer agent. The isolation of the dialdehyde product **4** was accomplished by both column chromatography (hexane:ethylacetate = 70:30) and recrystallization in methanol and water to give the desired product as a white solid. The ^{1}H-NMR of **4** (Figure 3.2) showed the singlet signal of hydroxylic proton at 11.44 ppm and aldehydic proton at 9.70 ppm indicating the incorporation of the salicylaldehyde group. The unusual upfield signal of the hydroxylic proton was attributed to the intramolecular H-bonding between the hydroxyl and the formyl groups. The number of signals and their integration well corresponded to the disubstitution of the tosyl groups onto the 2,4-dihydroxybenzaldehyde groups.

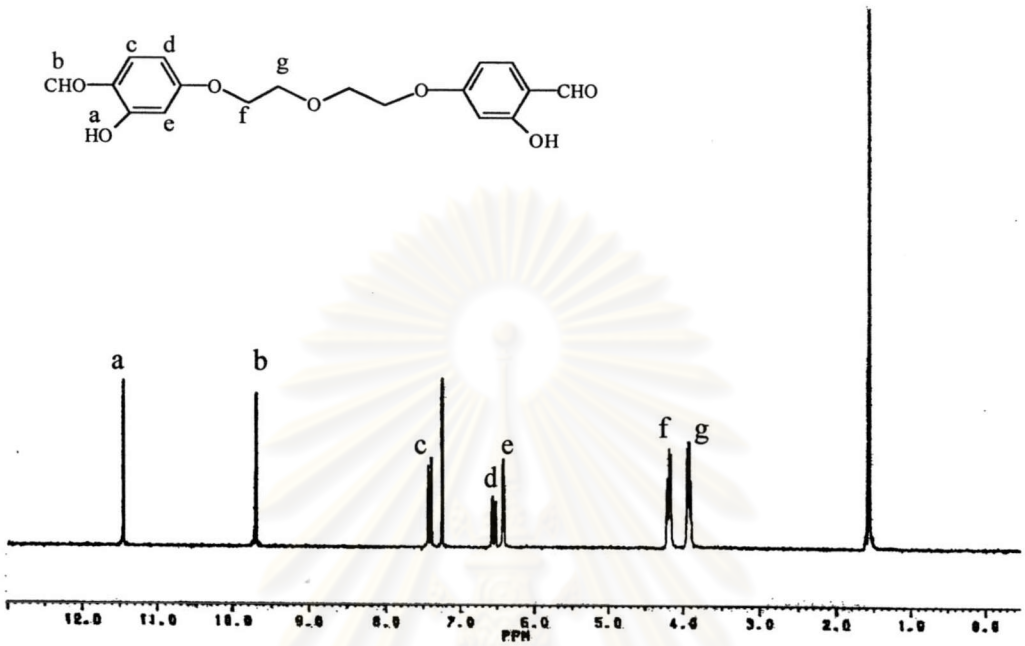

Figure 3.2 The ^{1}H-NMR spectrum of diethyleneglycol bis(4-salicylyl)ether, **4**

Product **5** and **6** were also synthesized and purified by the similar method to the dialdehyde **4**. However, the yield of product **6** was much poorer than those of the products **4** and **5**. The lower yield was due largely to the formation of mono- and trisubstituted products (**11** and **12**). These two undesirable products posted great difficulty in the isolation of the desired product **6**.

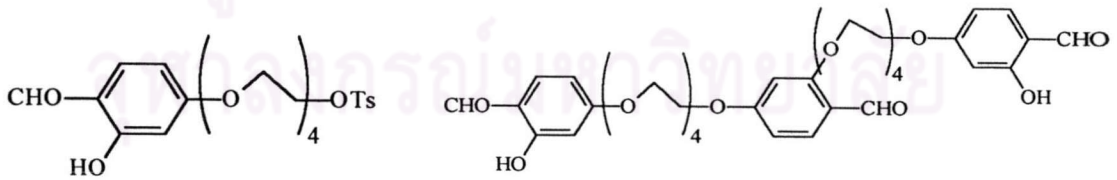

11 **12**

The polycondensation of the dialdehyde monomers (**4**, **5** and **6**) with (*R,R*)-1,2-diaminocyclohexane mono(+)tartate salt was carried out in two successive steps. In the first step, ethanol was used as a solvent to facilitate partial dissolution of the tartrate salt and K_2CO_3 base. Upon polymerization, yellow solid started to precipitate. When the precipitation became fully visualized, ethanol was evaporated off and THF was used in place as a solvent to increase the solubility of the polymers in the reaction. The solubility of the polymers was necessary for the polymerization to proceed toward higher molecular weight. The polycondensation yielded the desired polymer **7** in 79% yield.

The appearance of singlet signal of iminic proton at 8.01 ppm and the broad signal of cyclohexane proton at 1.40-3.16 ppm on ^{1}H-NMR spectrum together with the disappearance of singlet signal of aldehydic proton at 9.70 and confirmed the structure of polymer **7** (Figure 3.3). Furthermore, the broad peak of hydroxylic proton at 13.77 ppm resulted from the strong intramolecular H-bonding of the phenolic proton to the nitrogen atom of the imine group.

Tri- and tetraethyleneglycolic polymeric salens were also prepared in good yields (81% and 83% yields, respectively) by using the similar procedure.

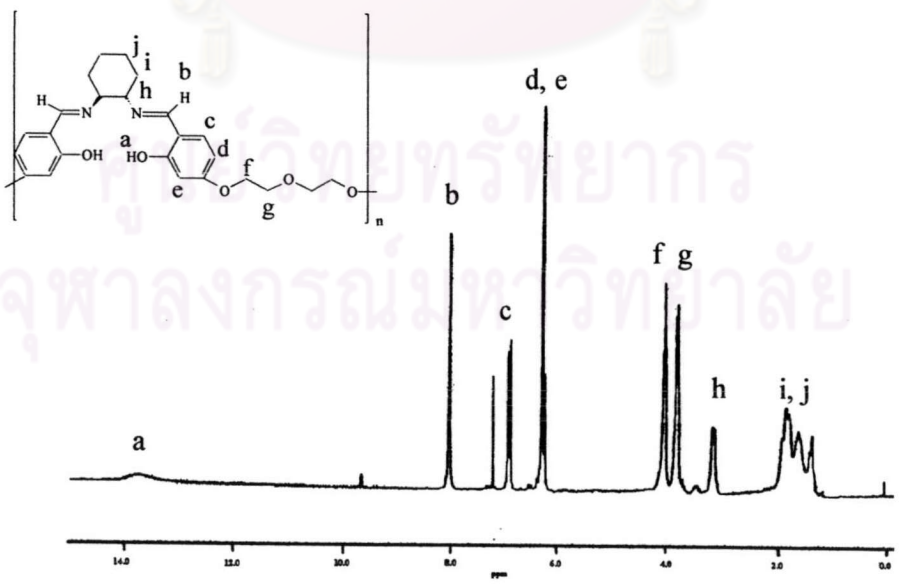

Figure 3.3 The ^{1}H-NMR spectrum of polymeric diethyleneglycol salen, **7**

3.2 Molecular Weight Determination

The molecular weight of all synthesized polymers were determined by both ^{1}H-NMR and GPC methods.

1. ^{1}H-NMR method.

The number average molecular weight (M_n) was calculated from the ratio of peak integration of the proton signal of the internal repeating unit over the peak integration of the proton signal of the terminal units (Table 3.1). The iminic proton signals of the internal repeating units at 8.00 ppm and the iminic proton signals of the terminal units at 8.20 ppm were utilized in the case where the chain termini were imine (Figure 3.4a). In the case where the chain termini were aldehyde (Figure 3.4b), the integration of aldehydic proton signals of the terminal units at 9.90 ppm were used as the nominator.

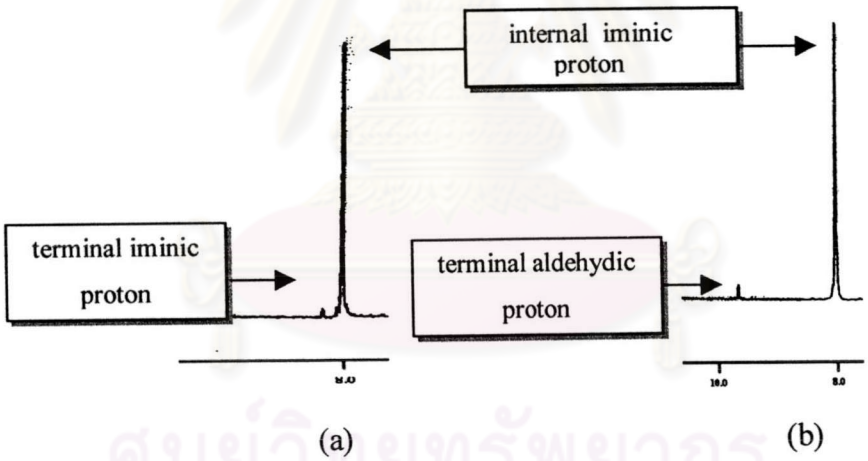

Figure 3.4 ^{1}H-NMR of 2 types of chain termini obtained from synthesized polymers.

2. GPC method.

GPC (Gel-Permeation Chromatography) is a very useful means for determination of both number and weight average molecular weight (M_n and M_w). The GPC analysis was carried out by using chloroform as a mobile phase at 25 °C, flow rate: 0.5 mL/min, detector: Jasco UV-970, λ: 275 nm. The molecular weight were obtained by using a calibration line from the polystyrene standards. Table 3.1 showed the results obtained from GPC.

Table 3.1 Molecular Weight of all polymers obtained from ^{1}H-NMR and GPC.

Polymer	Number of repeating units (rpu) from ^{1}H-NMR	GPC analysis		
		Number of rpu	M_n	M_w
$((EG)_2sal)_n$ (**7**)	27	12	5,100	12,300
$((EG)_3sal)_n$ (**8**)	21	11	5,250	9,980
$((EG)_4sal)_n$ (**9**)	-*	34	17,500	20,800

* ^{1}H-NMR of $((EG)_4sal)_n$ showed no proton signal of chain terminal at both 8.20 (iminic chain terminus) and 9.90 (aldehydic chain terminus) ppm.

From Table 3.1, the M_n of polymer **7** and **8** obtained from GPC was only one half of those obtained from NMR. The formation of cyclic oligomers (**13**) as part of the polymerization was a possible explanation of these differences[17,18]. These cyclic oligomers have no chain terminus. The number of repeating units obtained from ^{1}H-NMR were thus over estimated.

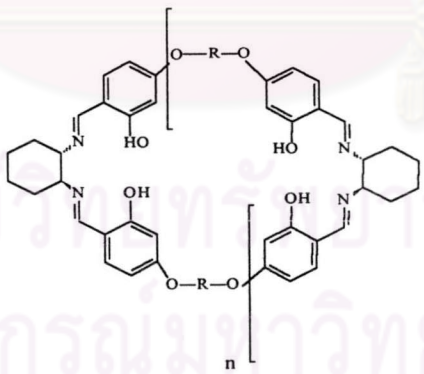

13

The ^{1}H-NMR signal of polymer **9** showed no observable signal of the chain terminus implying a high molecular weight of the polymer. The GPC results also showed that M_n of polymer **9** was about three times higher than those of polymers **7** and **8**. However, later synthesis of polymer **7** and **8** also showed no observable signal of the chain terminus on ^{1}H-NMR indicating the high molecular weight of these polymers. We thus did not think that the differences in the molecular weights observed in the earlier results (Table 3.1) were caused by the differences in the length of ethyleneglycolic chains.

3.3 The complexation studies and their solubility tests

The complexation reaction of synthesized polymers with various metal ions was performed by reacting 1 equivalent of polymer with 1.1 equivalents of metal solution in the presence of 2.6 equivalents of CH_3COONa as a base. The color of the polymeric solution was immediately changed upon the addition of each metal solution inferring the occurrence of the complex. Table 3.2 showed the color of metal salen complexes.

Table 3.2 The color of synthesized metal salen complexes.

Metal ions	Color of complexes
Ni^{2+}	Red
Co^{2+}	Brown
V^{4+}	Green
Mn^{2+}	Brown

The solubilities of all complexes were examined in various solvents (Table 3.3). All metal complexes obtained from polymeric diethylene glycolic salen were not soluble in any organic solvents. This result implied that the flexibility of diethylene glycolic chain incorporated into the polymers was insufficient to overcome the rigidity of the metal-salen building block. The longer glycolic chains, tri- and tetraethylene glycolic chain, were expected to increase the flexibility of the polymeric complexes and thus the solubility. Indeed, the complexes of polymeric tri- and tetraethylene glycolic salen, excepted for the cobalt complexes, were soluble in some solvents. The insolubility was first thought to be due to crosslinking since cobalt contains add electrons and can acquire an additional electron through bridging. However, the cobalt salen complex was soluble in some solvents when the complex was prepared by using 0.6 equivalent of the cobalt ion reacted with 1 equivalent of the polymer. Therefore, it is not likely that the insolubility of complexed polymer was due mainly to the crosslinking since the partially complexed polymer was soluble. At the presence, we have no definite explanation for the fully cobalt complexed polymer.

Table 3.3 The solubility tests of all metal salen complexes.

Complexes	Solvent (low → Polarity → high)						
	Hexane	CH_2Cl_2	$CHCl_3$	EtOAc	DMF	H_2O	MeOH
$(V\text{-}(EG)_2sal)_n$	✗	✗	✗	✗	✗	✗	✗
$(Mn\text{-}(EG)_2sal)_n$	✗	✗	✗	✗	✗	✗	✗
$(Co\text{-}(EG)_2sal)_n$	✗	✗	✗	✗	✗	✗	✗
$(Ni\text{-}(EG)_2sal)_n$	✗	✗	✗	✗	✗	✗	✗
$(V\text{-}(EG)_3sal)_n$	✗	✓	✓	✗	✓	✗	✗
$(Mn\text{-}(EG)_3sal)_n$	✗	✓	✓	✗	✓	✓	✓
$(Co\text{-}(EG)_3sal)_n$	✗	✗	✗	✗	✗	✗	✗
$(Ni\text{-}(EG)_3sal)_n$	✗	✗	✗	✗	✗	✗	✗
$(V\text{-}(EG)_4sal)_n$	✗	✓	✓	✗	✓	✗	✗
$(Mn\text{-}(EG)_4sal)_n$	✗	✓	✓	✗	✓	✓	✓
$(Co\text{-}(EG)_4sal)_n$	✗	✗	✗	✗	✗	✗	✗
$(Ni\text{-}(EG)_4sal)_n$	✗	✓	✓	✗	✗	✗	✗

✓ = soluble , ✗ = insoluble

The ^{1}H-NMR of all soluble complexes were acquired. However, due to the paramagnetism of the transition metal ions, the spectra contained very broad signals that did not enable the determination of degree of the complexation. Therefore, the determination of the degree of complexation was investigated by Atomic Absorpsion Spectroscopy (AAS). The results confirmed the incorporation of metal ions into polymeric structure (Table 3.4). The difference in the degree of complexation between nickel and manganese complexes probably resulted from the geometry constrain of the manganese complex.

Table 3.4 Degree of complexation obtained from AAS

Polymeric salen complexes	% of metal ions
$(Ni\text{-}(EG)_4sal)_n$	100
$(Mn\text{-}(EG)_4sal)_n$	37

3.4 Electrochemical Studies

3.4.1 The studies of the effect of electrolyte

The electrochemical properties in both aqueous and non-aqueous system of the synthesized polymer complexes were studied by using cyclic voltammetry.

In aqueous solution, metal salen complex was coated on a Pt working electrode and the cyclic voltammetry was performed at the scan rate of 0.2 mV/s using PBS solution pH 7.4 as a buffer. Under the aqueous condition, there were no voltammetric peaks when all modified electrode was measured in PBS solution. Figure 3.5 showed the voltammogram of $(Ni\text{-}(EG)_4sal)_n$ modified electrode comparing with that of Pt electrode in PBS solution as an example.

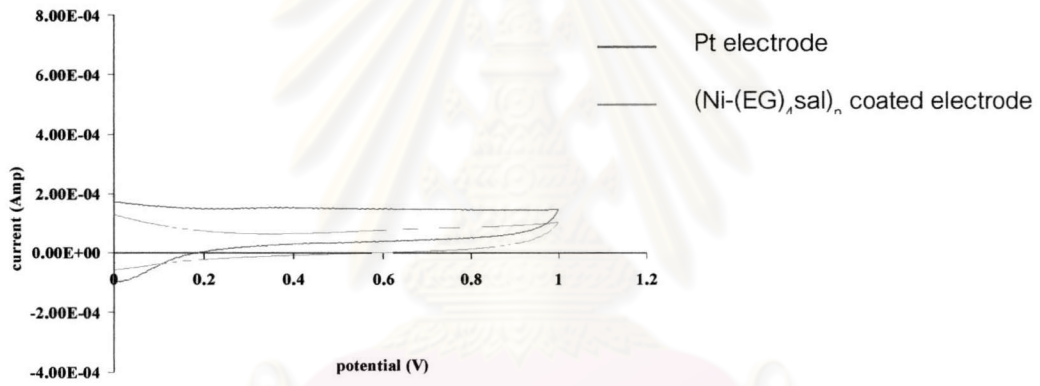

Figure 3.5 Voltammogram of Pt and $(Ni\text{-}(EG)_4sal)_n$ coated electrode.

The absence of the signal of metal-salen complex films may be attributed to the slow rate of charge propagation into the polymer film from the aqueous medium[3].

In acetonitrile, all selected complexes showed signals (Table 3.5) corresponding to the oxidation of metal ions[3,19].

Table 3.5 The redox potential of all complexes in non-aqueous solution.

Complexes	Potential (V)		Chemical reaction
	E_{ox}	E_{red}	
$(Ni\text{-}(EG)_4sal)_n$	0.65	0.38	Quasi-reversible
$(V\text{-}(EG)_4sal)_n$	0.23	-	Irreversible
$(Mn\text{-}(EG)_4sal)_n$	0.60/1.01	-	Irreversible

Although all complexes showed the voltammetric signals in non-aqueous condition, only the signal obtained from nickel complexes manifested redox peaks (Figure 3.6). Further investigation was thus base on the $(Ni\text{-}(EG)_4sal)_n$ coated electrode unless stated otherwise.

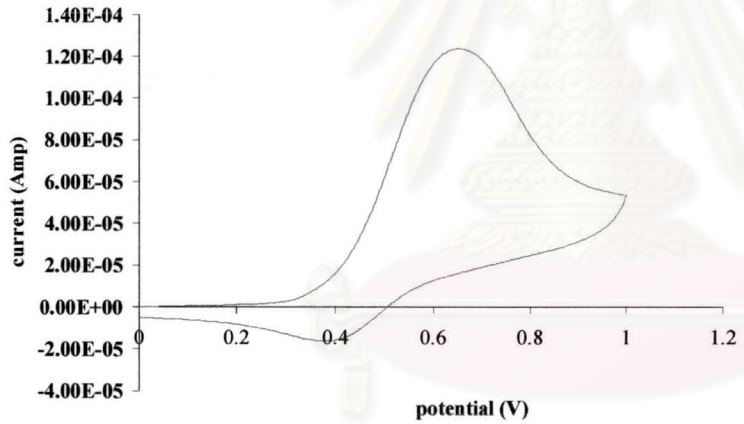

$(Ni\text{-}(EG)_4sal)_n$ coated electrode

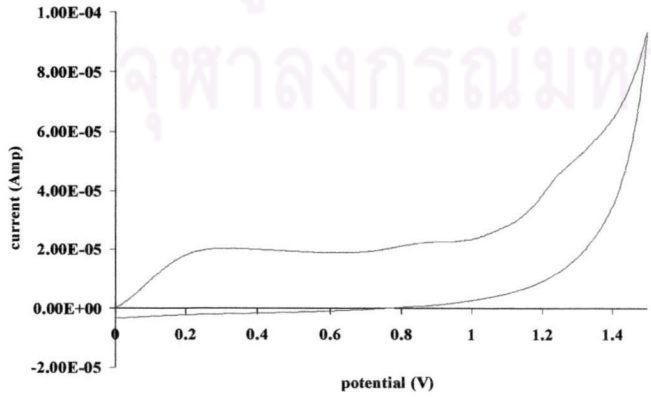

$(V\text{-}(EG)_4sal)_n$ coated electrode

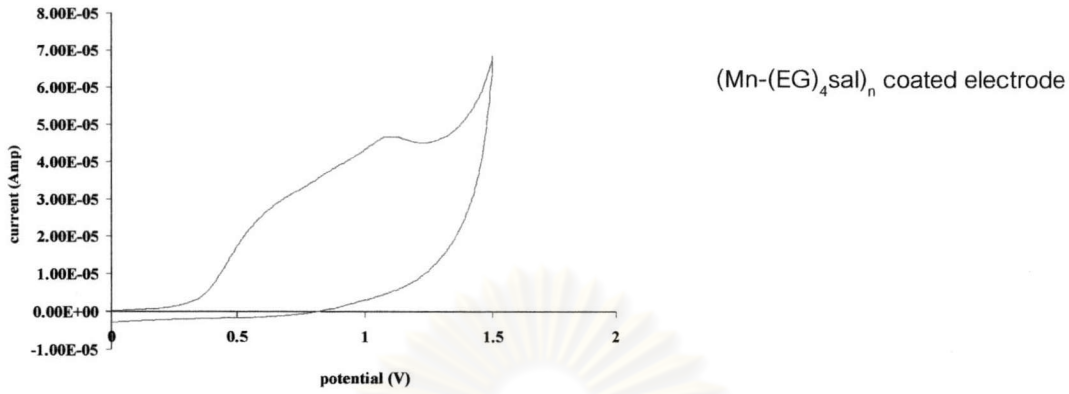

Figure 3.6 Voltammograms of metal-salen complexes modified electrode.

The redox signals of the $(Ni\text{-}(EG)_4sal)_n$ coated electrode were diminished on the repetitive scans. The decrease of the current indicate the decrease of the amount of electroactive Ni^{2+} species remained on the surface of modified electrode presumably due to the non-reversible adsorption phenomenon. The similar event was also observed when modified electrode was used to detect some analytes. The discussion of this experiment would thus be explained afterward.

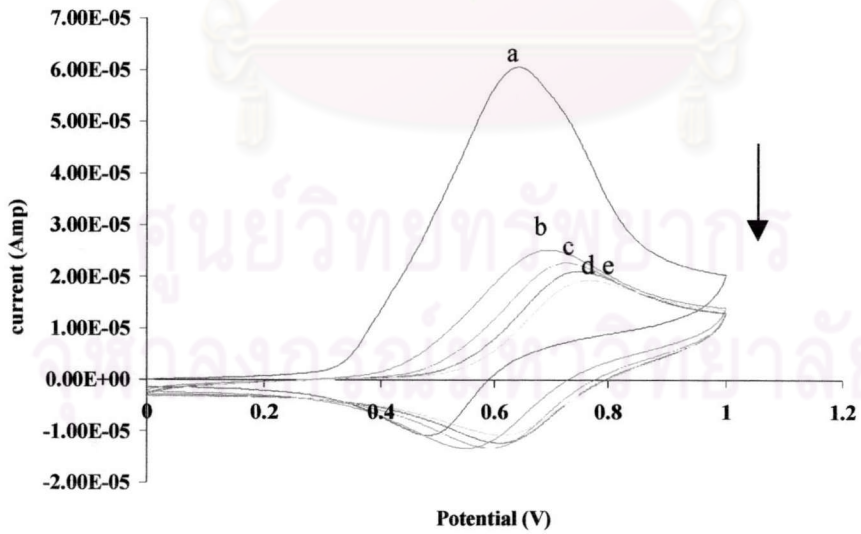

Figure 3.7 The voltammogram of $(Ni\text{-}(EG)_4sal)_n$ modified electrode with (a) 1st , (b) 5th , (c) 10th, (d) 15th and (e) 20th scan.

3.4.2 The sensitivity of metal-salen modified electrode to selected organic compounds.

As a tetradentate ligand, salen normally occupies four coordination sites on metal ions leaving one or two coordination sites for more labile ligands. Any organic compounds containing lone pair electrons may act as a labile ligand interacting with the metal-salen complex at these free sites. This interaction should bring about certain degree of disturbation on the electronic potential of the metal complex. First, the $(Ni\text{-}(EG)_4sal)_n$ modified electrode was used in a preliminary test for sensoring of pyridine. The cyclic voltammetry was performed in the non-aqueous electrolyte with (2.48×10^{-1} M) and without pyridine. The voltammogram (Figure 3.8) displayed the anodic peak of the solution containing pyridine at 0.48 V shifted from the peak of solution without pyridine (0.66 V). Moreover, the cathodic wave of the modified electrode was disappeared when the cyclic voltammetry was performed in the presence of pyridine.

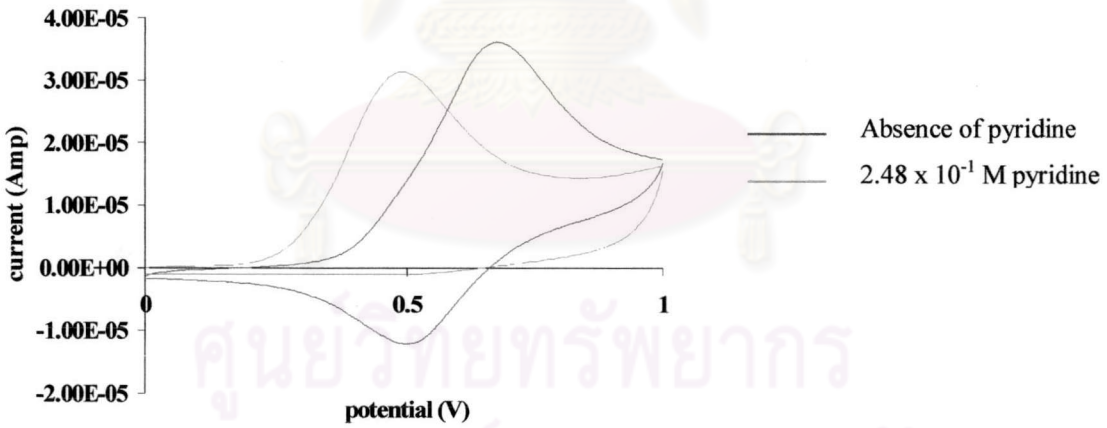

Figure 3.8 The cyclic voltammogram in the free electrolyte and electrolyte containing 2.48×10^{-1} M pyridine using $(Ni\text{-}(EG)_4sal)_n$ as working electrode.

In successive addition of pyridine, the decreasing in magnitude of the current was also observed together with the shift of the potential. This result implied that the interaction between pyridines and nickel central ions affected the electronic property of $(Ni\text{-}(EG)_4sal)_n$ that led to the shift of the anodic signal. Moreover, the disappearance of the cathodic signal was also observed in the first scan (Figure 3.8).

The following electrochemical process was purposed to explain all of the observation. Obtained from the oxidation of the $(Ni\text{-}(EG)_4sal)_n$ coated electrode, Ni^{3+} species, due to their instabilities, would acquire an electron from pyridine and were then converted to more stable Ni^{2+} species. The generated reactive pyridine radical cation would be likely to polymerize to give polymer film covering the surface of the modified electrode. This adsorption effectively obstructed further electrochemical reaction at the central ion resulting in the disappearance of the cathodic wave. The disappearance of both oxidative and reductive signals in the next scan (Figure 3.9) were also supported the non-reversible adsorption hypothesis. Moreover, this non-reversible adsorption of the generated polymeric materials on the surface of the electrode may also well explain the diminishing of oxidative signal observed in the voltammetric experiment in the absence of pyridine. In the absence of pyridine, acetonitrile, used as a solvent, may serve as an electron donor but to the lower extent than pyridine. The signals were just diminished but remained observable.

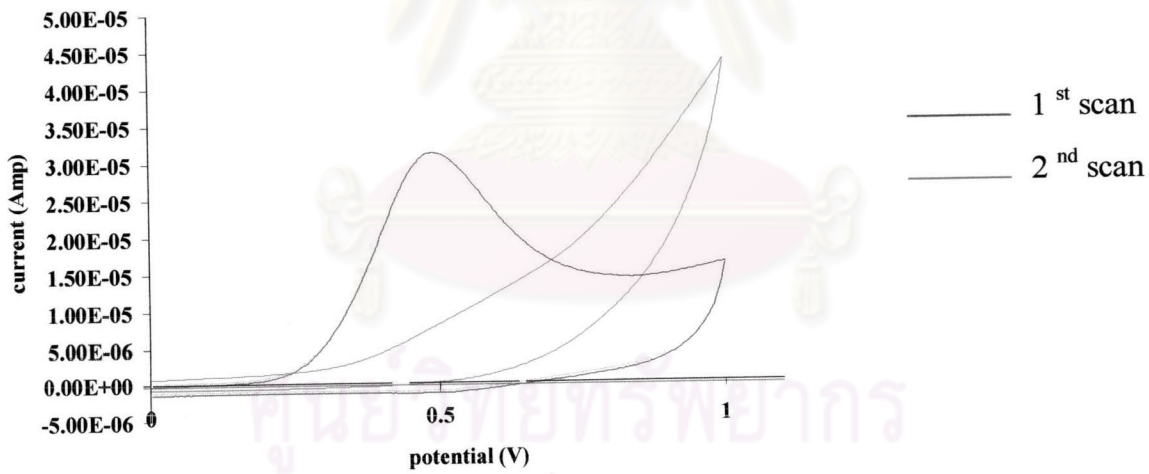

Figure 3.9 The voltammogram of $(Ni\text{-}(EG)_4sal)_n$ modified electrode in the presence of 2.48×10^{-1} M pyridine on the repetitive scan.

To verify adsorption hypothesis, the modified electrode was sonicated in distilled water for 5 minutes and then dried under purging N_2. The voltammogram of this sonicated electrode (Figure 3.10) showed almost full recovery of the oxidation current. This result indicated that sonication was rather efficient for desorbing adsorbed polymeric materials on the surface of the modified electrode.

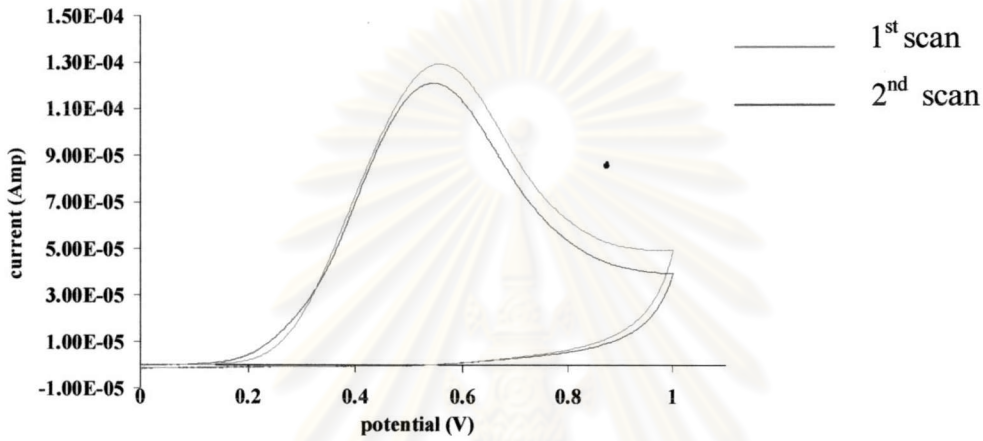

Figure 3.10 The voltammogram of recycle $(Ni\text{-}(EG)_4sal)_n$ modified electrode in electrolyte containing 1.24×10^{-1} M pyridine.

Moreover, the amount of pyridine (2.48×10^{-1} M) could not be detected by using a glassy carbon working electrode (Figure 3.11). Therefore, in comparison with the voltammogram obtained from $(Ni\text{-}(EG)_4sal)_n$ coated electrode, the modification of our metal-salen complexes on the surface of glassy carbon electrode could enhance the sensitivity of the electrode to the pyridine.

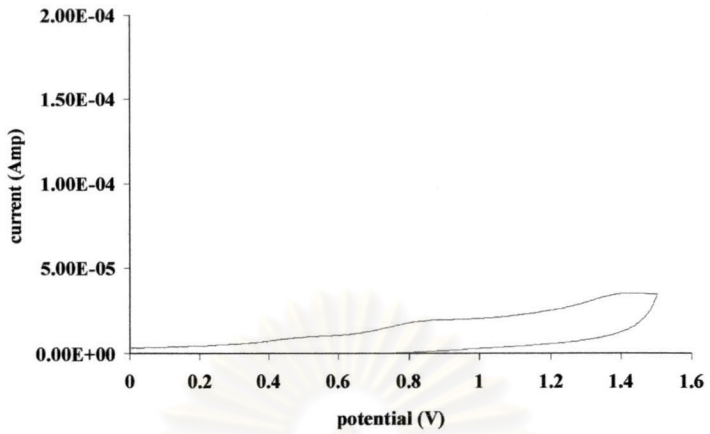

Figure 3.11 The voltammogram of glassy carbon electrode in the presence of 2.48 x 10^{-1} M pyridine

Other organic compounds containing lone pair electron such as styrene oxide, methanol and methylbenzylamine were also used as analytes in the preliminary tests. The shift of the oxidation signal and the disappearance of the cathodic wave were also observed when the modified electrode was placed in non-aqueous electrolyte containing 1.76 x 10^{-1} M styrene oxide and 4.97 x 10^{-1} M methanol (Figures 3.12 a and b). The shift of the oxidation signal for styrene oxide and methanol was ,however, not as distinctive as what was observed in the case of pyridine.

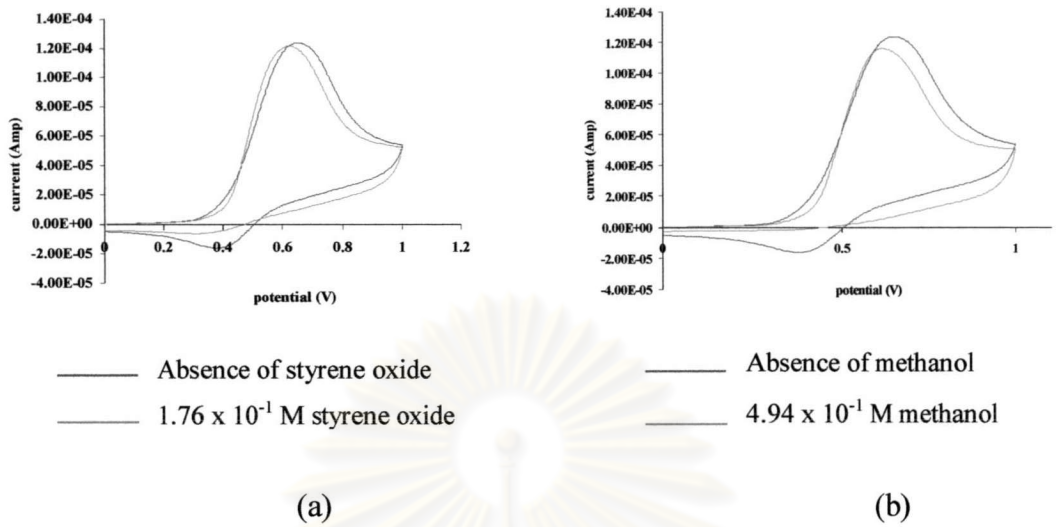

Figure 3.12 The voltammogram in the absence and presence of (a) styrene oxide, (b) methanol.

Unlike other analytes, the voltammogram of nickel salen modified electrode in electrolyte containing 100 μL methylbenzylamine (7.86×10^{-2} M) showed 2 oxidation peaks at 0.42 and 0.80 V assumingly corresponding to the oxidation signals of Ni^{2+} and methylbenzylamine respectively (Figure 3.13).

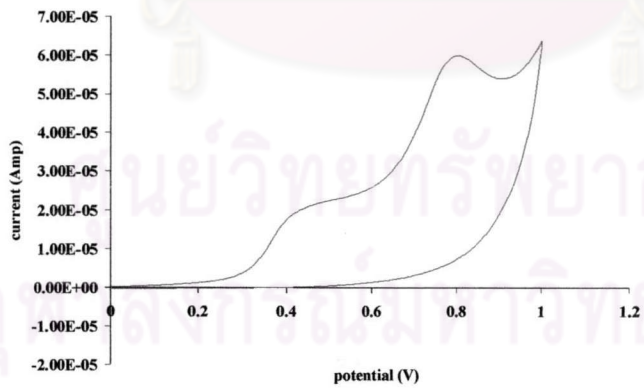

Figure 3.13 The cyclic voltammogram of $(Ni\text{-}(EG)_4sal)_n$ modified electrode in the presence of 7.86×10^{-2} M methylbenzylamine.

The difference in the anodic shift of all analytes, at the similar concentration, implied the different sensitivity of the $(Ni\text{-}(EG)_4sal)_n$ coated electrode toward each analytes (Table 3.6).

Table 3.6 The concentration and potential shift of all analytes detected by $(Ni\text{-}(EG)_4sal)_n$ modified electrode.

Analytes	Concentration (M)	Potential shift (V)
Methanol	4.94×10^{-1}	0.04
Styrene oxide	1.76×10^{-1}	0.02
Pyridine	2.48×10^{-1}	0.18
Methylbenzylamine	7.86×10^{-2}	0.23

The largest shift that was observed in the voltammogram of electrolyte containing 7.86×10^{-2} M methylbenzylamine resulted from the strongest basicity of the methylbenzylamine.

The methylbenzylamine was appeared to be oxidized at $(Ni\text{-}(EG)_4sal)_n$ modified electrode and thus two signals were obtained. To simplify the result, $(Mn\text{-}(EG)_4sal)_n$, which showed much lower in the magnitude of current in free electrolyte, was selected to replace the $(Ni\text{-}(EG)_4sal)_n$ electrode in the sensoring test of methylbenzylamine. The cyclic voltammogram of $(Mn\text{-}(EG)_4sal)_n$ modified electrode showed only one oxidation peak at 1.14 V in 3.93×10^{-2} M methylbenzylamine. Additionally, the increasing of the current was observed proportional to the concentration of analyst (Figure 3.14).

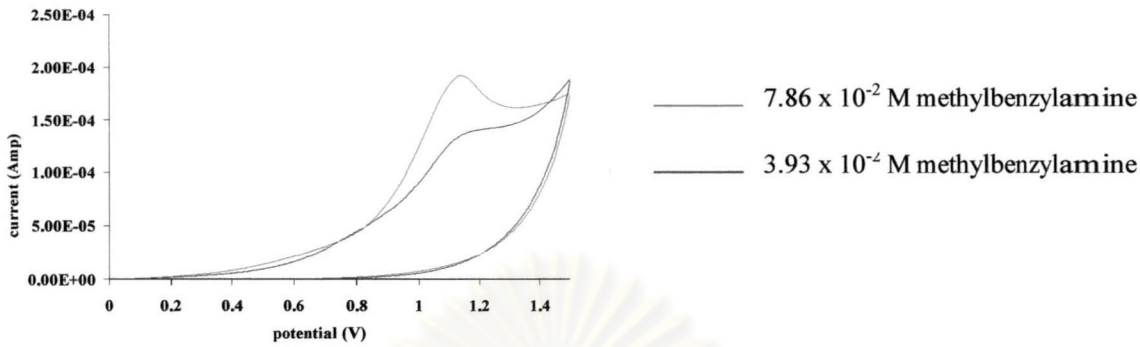

Figure 3.14 Cyclic voltammogram of $(Mn(EG)_4sal)_n$ modified electrode in the presence of methylbenzylamine at different concentration.

The cyclic voltammetry in electrolyte containing methylbenzylamine using glassy carbon as working electrode was performed for comparison (Figure 3.15). The methylbenzylamine could be oxidized at the $(Mn\text{-}(EG)_4sal)_n$ modified electrode at the similar potential and with a higher oxidation current compared with that of at the unmodified glassy carbon electrode, suggesting that $(Mn\text{-}(EG)_4sal)_n$ modified electrode showed the higher sensitivity toward methylbenzylamine than unmodified glassy carbon electrode.

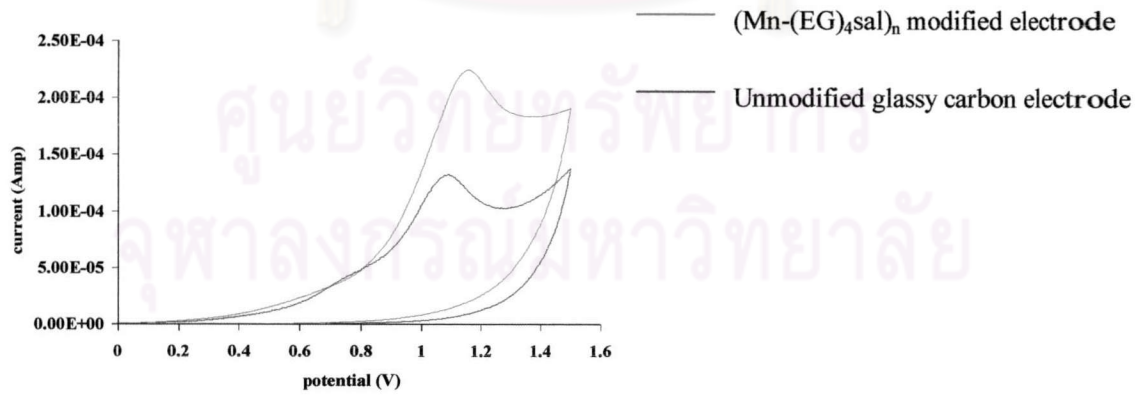

Figure 3.15 Cyclic voltammogram in electrolyte containing 7.86 x 10^{-2} M methylbenzylamine using a different working electrode.

Furthermore, our metal salen complexes contain chiral center which probably can interact differently between 2 enantiomers and thus the difference in the magnitude of the shift of the voltammetric signals. The detection of chiral organic compounds were thus also prompt our interests. The (*R,R*) and (*S,S*)-1,2-diaminocyclohexane were used as the model chiral organic compounds detecting by $(Ni\text{-}(EG)_4sal)_n$ coated electrode. The voltammogram of electrolyte containing 1×10^{-3} M (*R,R*) and (*S,S*)-1,2-diaminocyclohexane, however, displayed similar potential implying the chiral center in our complex was insufficient to distinguish the binding of the different enantiomers of the analytes (Figure 3.16).

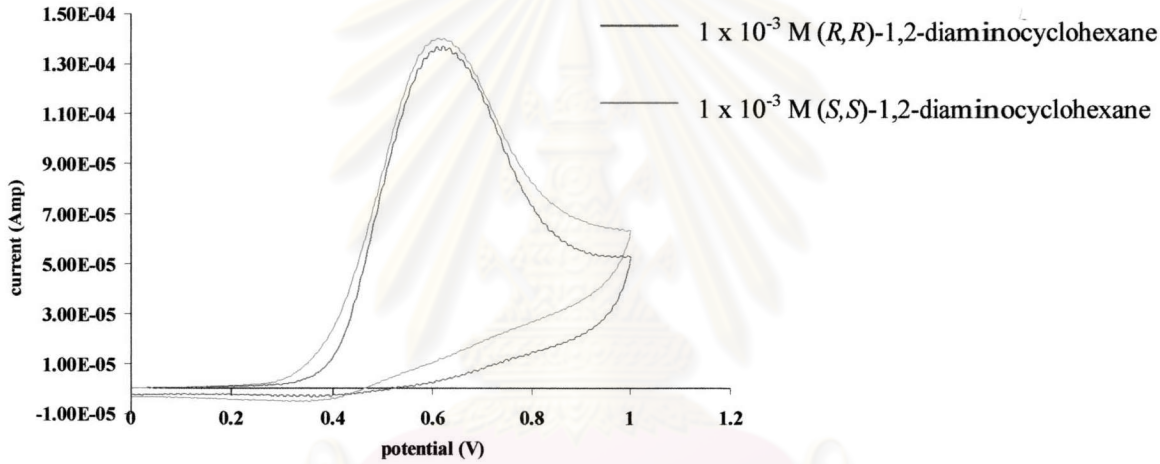

Figure 3.16 Cyclic voltammogram in electrolyte containing (*R,R*) and (*S,S*)-1,2-diaminocyclohexane using $(Ni\text{-}(EG)_4sal)_n$ as working electrode.

3.4.3 The linear range of modified electrode to the analytes

For quantitative analysis, selected analytes were tested to find out the linear range toward metal-salen modified sensor. First, the linear range of pyridine was measured from the shift of oxidation peak of Ni^{2+} signal resulting from the successive addition of the pyridine in acetonitrile containing TBAP by using nickel salen coated electrode as working electrode. The potential shift were proportional to the concentration of pyridine within the range from 2.48 x 10^{-2} to 1.48 x 10^{-1} mol/L (Figure 3.17).

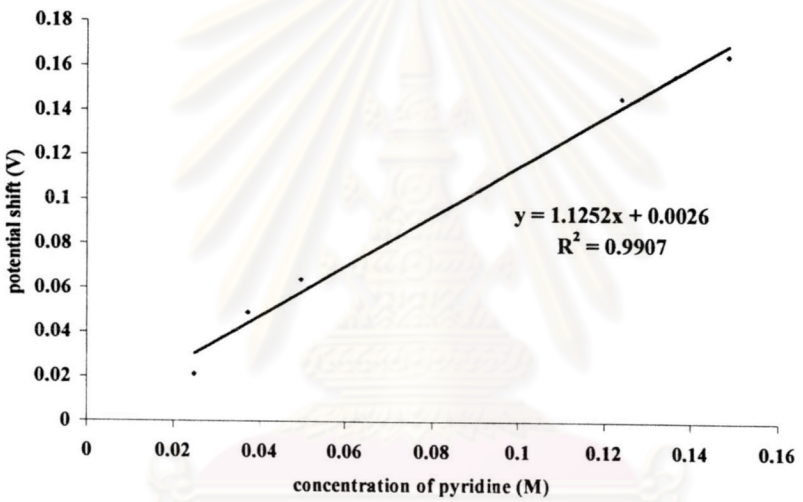

Figure 3.17 The plot between the potential shift and the concentration of pyridine.

The linear range of (*R,R*) and (*S,S*)-1,2-diaminocyclohexane were also measured with the similar method and found that the linear range of both analytes were in the range from 1.00 x 10^{-3} to 5.00 x 10^{-3} M (Figures 3.18 a and b).

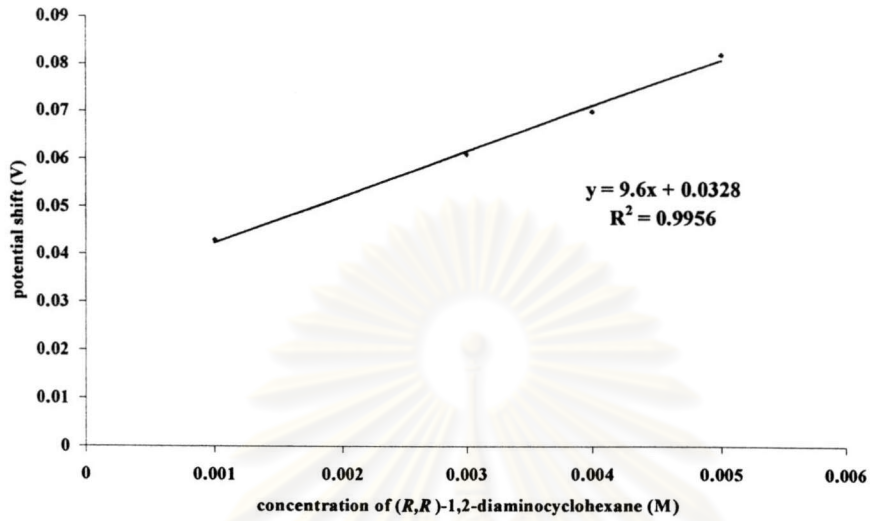

(a)

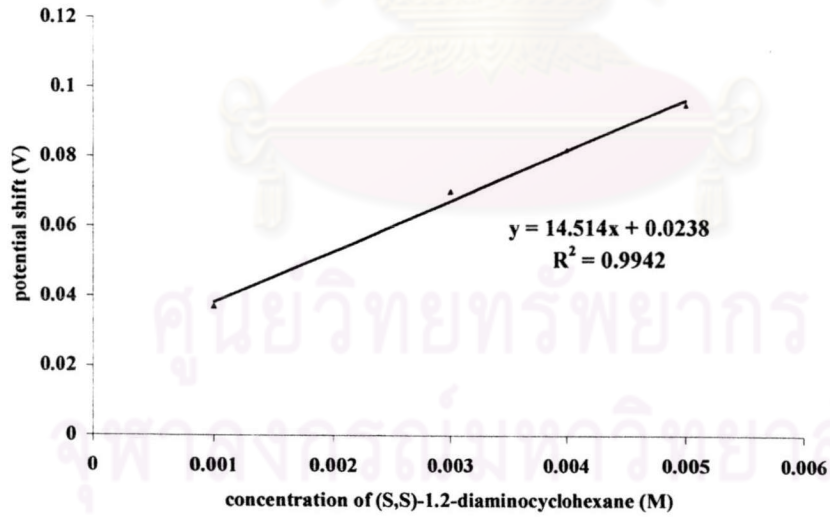

(b)

Figure 3.18 The plot between the potential shift and the concentration of (a) (*R,R*)- and (b) (*S,S*)-1,2-diaminocyclohexane.

As mentioned earlier, methylbenzylamine was measured by using $(Mn\text{-}(EG)_4sal)_n$ modified electrode. The linear range of this analyte was determined from the oxidation current of the methylbenzylamine resulting from the successive addition of the methylbenzylamine in acetonitrile containing TBAP. The oxidation currents of the electrode were proportional to the concentration of methylbenzylamine within the range from 2.36×10^{-2} to 5.50×10^{-2} mol/L (Figure 3.19).

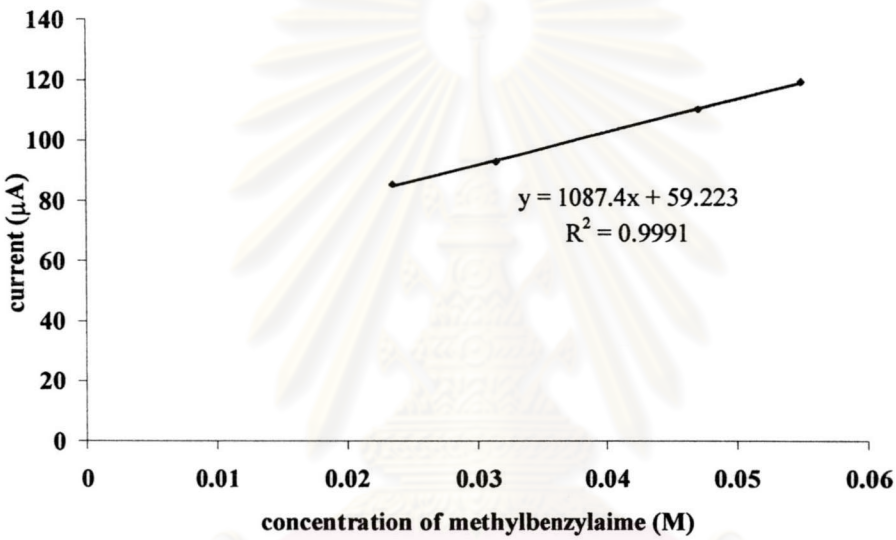

Figure 3.19 The plot between the current and concentration of methylbenzylamine.